[Downloaded free from http://www.toxicologyinternational.com on Monday, October 10, 2016, IP: 115.115.223.222]

Original Article

Dose Dependent Effect of Iso-Octane on HaCaT: A Model Study

Lopamudra Das, Soumen Das, Jyotirmoy Chatterjee

School of Medical Science and Technology, Indian Institute of Technology, Kharagpur, West Bengal, India

ABSTRACT

Objective: Improved understanding of cytotoxicity under chemical assaults may be achieved by multimodal analysis of cellular morphology, viability, molecular expressions, and biophysical properties. **Materials and Methods:** In this study dose-dependent effects of an organic solvent (OS), iso-octane (IO), known to cause skin irritation, has been explored multimodally for understanding its effect on structural and functional profile of normal epithelial cell population *in vitro*. **Results:** Under IO exposures, after 5 h there was a sharp decrease in viability of HaCaT with increasing doses which may be due to disruption in cellular association noted via immunocytochemical study and was further supported by the decreased expression of E-cadherin at transcriptomic level. Dislocation of E-cadherin from membrane to the cytoplasm occurred with increasing doses. The dose-dependent changes in varied aspects of bioelectrical properties, having plausible correlation with cellular viability, association, and adherence were noteworthy at 5 h of IO exposure. Evaluation of biomechanical properties by micropipette aspiration showed a distinct change in cellular stiffness in terms of increase in suction force and post-suction alteration in cellular shape. The cells became stiffer and fragile with increasing IO doses. **Conclusion:** Present study explicated dose–dependent cytotoxicity of IO on HaCaT and explored the usefulness of this approach to develop *in vitro* model system to evaluate epithelial toxicity with level-free markers.

Key words: Biomechanical property, cytotoxicity, E-cadherin, electrical impedance, iso-octane

INTRODUCTION

Excessive chemicals usage in modern times is a reason for threat to both the health and environment. The number of synthetic substances to which humans are exposed has increased tremendously over the last decades.[1] In the context of hazards, toxic effect of OSsis a major health concern,[2] especially due to their cytotoxicity[3] and protein denaturing effects.[3,4] IOis one of the synthetic OS which needs attention particularly to reveal its impact on mammalian objects. It is produced in a considerable amount in the petroleumindustry[5] and is one of the important components of gasoline too. IO is also used for production of ethanol with extremely low volatility.[6] In spite of its profuse usage worldwide, IO is reported to be toxic and a potent skin irritant on exposure. It has also been reported to have effects on aquatic life when released in seas or rivers.

The degree of toxicity of OS is dependent on the cell type and its physiological status.[7] Cytoplasmic membrane acts as the primary site of cellular cytotoxic action.[4] Cytotoxicity

Address for correspondence: Dr. Lopamudra Das, Department of Materials Engineering, Indian Institute of Science Bangalore - 560 012, Karnataka, India.
E-mail: lopamudra.das.iitkgp@gmail.com

Access this article online

Quick Response Code:

Website: www.toxicologyinternational.com

DOI: 10.4103/0971-6580.172264

This is an open access article distributed under the terms of the Creative Commons Attribution-NonCommercial-ShareAlike 3.0 License, which allows others to remix, tweak, and build upon the work non-commercially, as long as the author is credited and the new creations are licensed under the identical terms.

For reprints contact: reprints@medknow.com

How to cite this article: Das L, Das S, Chatterjee J. Dose dependent effect of Iso-Octane on HaCaT: A model study. Toxicol Int 2015;22:83-91.

© 2015 Toxicology International | Published by Wolters Kluwer - Medknow

[Downloaded free from http://www.toxicologyinternational.com on Monday, October 10, 2016, IP: 115.115.223.222]

of IO on microorganism like yeast has already been reported,[8] but its impact on the mammalian cells is not well-documented. In the context of its irritating effects on skin, vulnerability of epithelium in the development of 90% cancers was already reported.[9] Multimodal understanding of IO's effects on cells of epithelial origin, namely HaCaT (normal keratinocyte) may be important, especially to reveal its effects on structural and functional integrity of cells.[10] The correlated assessment of changes in the cellular viability, molecular expressions as well as bioelectrical and biomechanical properties are gaining importance[11] in the multidimensional study. The cell viability assay provides useful information on the cytotoxic effect of a chemical.[12] The cells under assaults become stressed, resulting in an altered functioning affecting the morphological features and cell–cell association.[13] In the milieu of epithelial cell–cell association, expression of E-cadherin by keratinocyte in confluence is important[14] and the change in membranous expression of this protein brings jeopardy in epithelial integrity.[15]

The studies on alteration in bioelectrical properties of cells under assaults[16] is important in the evaluation of cytotoxicity.[17] A living biological cell being electrically neutral generates electromotive force (EMF) to maintain potential difference[18] in modulating current flow[19] and at different functional and adhered conditions, exhibit changes in membrane potential, impedance, charge distribution, etc.[20,21] Thus, investigation of cellular electrical behavior when subjected to chemical assaults is useful to understand the alteration in functionality and viability.[22,23] In general, label free dielectric spectroscopic measurement on cell suspension is somewhat simple, noninvasive, and real-time technique. It provides crucial information about cell proliferation, morphology, and motility.

An increase in impedance with the formation of epithelial sheet due to cell–cell adhesion, proliferation, and spreading has already been reported.[20,24,25] The effect of E-cadherin regulation in real time was measured using electric cell-substrate impedance sensing (ECIS) to study the alterations in the epithelial resistance.[16,24] Increased epithelial resistance reflected the establishment of compact cell–cell adhesion in the confluent monolayer restricting current flow between neighboring cells. The study of mechanical properties of living cells helps in understanding their response when exposed to different physical and chemical stresses.[26] It is reported that the cells behave differently when exposed to stress both *in vivo* and *in vitro*.[27] Researches were conducted to characterize the response of cells to an applied pressure to study the flow behavior of the cells through the smallest vessels of the body for migration within tissue to the site of infection.[28] The cellular stiffness alteration in disease condition and under chemical assaults is well-documented.[29] The study of biomechanical properties of cells by micropipette aspiration is one of the methods adopted to understand the material properties of living cells. In this study, biomechanical signature helps in highlighting the biophysical changes in the cell line when exposed to different IO doses. Elastic properties of the normal cells[30] change substantially when they are treated with different concentrations of IO.

In this paper the effect of different doses of IO was studied on HaCaT cell line to record the changes in their structure, viability, and prime molecular expression along with changes in electrical impedance under the influence of an electric field on ECIS device and biomechanical property with micropipette suction method. Attempts have been made to correlate the observations to assess the cytotoxicity of IO doses.

MATERIALS AND METHODS

Materials

Immortal human skin keratinocytes, HaCaT cell line was obtained from National Centre for Cell Science, Pune, Maharashtra, India. Fetal bovine serum (FBS), DMEM-F12, antimycotic antibiotic, L-glutamine, and 0.05% trypsin-ethylenediaminetetraacetic acid (EDTA) solution, phosphate buffered saline (PBS), 3-(4,5- dimethylthiazol-2-yl)-2, 5-diphenyl-2H- tetrazolium bromide (MTT) salt, and HiPure kit were collected from Himedia (India); IO was from Merck (Germany); live-dead cell assay kit was from Invitrogen (Frederick, MD); High-Capacity cDNA Reverse Transcription Kit (Applied Biosystems, USA); iQ™ Sybr® Green Supermix (BioRad, CA, USA); goat serum, E-cadherin, and goat polyclonal to rabbit IgG (Abcam, UK); and DAPI (Sigma-Aldrich, USA).

Cell culture and treatment

HaCaT was seeded in concentration of 10^5cell/ml in Dulbecco's Modified Eagle'sMedium (DMEM) F12 supplemented with 10% FBS, 1% L-glutamine, and 1% antibiotics. Cells were cultured in 25 cm^2 culture flasks in a humidified incubator at 37°C with 5% CO_2 for 4 days to achieve confluence (~10^6 cells/ml) population. The HaCaT population was then incubated for 5 h with 5ml medium as the final volume containing 4% (200 µl), 6% (300 µl), and 8% (400 µl) of IO; and subsequently the effects were studied multimodally. Cell without IO exposure served as control (0%).

Phase contrast microscopy

HaCaT cell was grown to confluence using DMEM F12 medium and then treated with different IO doses for 5 h. The PCM of both control and experimental (treated with IO doses) groups of HaCaT were performed to identify

[Downloaded free from http://www.toxicologyinternational.com on Monday, October 10, 2016, IP: 115.115.223.222]

the visible morphological changes on IO treatment. The digital images (1,388 × 1,040 pixels) were taken by charge-coupled device (CCD) camera (AxioCam MRm) in phase-contrast mode of Zeiss observer microscope (model Z1, Carl Zeiss, Germany), under × 10 objective (numerical aperture (NA) 0.25 with 0.63 μm resolution).

MTT assay

In the determination of mitochondrial function and cell viability of HaCaT after 5 h treatment under different IO doses, cells were incubated with MTT (Himedia, India) according to the manufacturer's protocol. Three replicates for each IO doses were examined. Absorbance values at 570 nm for MTT were measured using a microplate spectrophotometer (Bio-RAD Benchmark Plus).

Relative quantification of gene expression through reverse transcription polymerase chain reaction

Preparation of cells for ribonucleic acid (RNA) isolation

HaCaT cells in confluence were exposed to different doses of IO for 5 h and cells without IO exposure served as the control group. After IO exposure the cells were trypsinized and centrifuged for 5 min at 5,000 rpm to obtain the cellular pellet to be used for RNA isolation. Similar method was adopted to prepare the samples for bio-impedance study.

RNA isolation and complementary deoxyribonucleic acid (cDNA) conversion

Total RNA was extracted from cells of both control and experiments with 10^6 cell/ml concentration using HiPure kit (HiMedia, India) and according to the manufacturer's protocol. The extracted RNA was checked for both quantity and quality using spectrophotometer at 260 and 280 nm and also by agarose gel electrophoresis. Reverse transcription reaction was performed using 1 μg of RNA with High-Capacity cDNA Reverse Transcription Kit (Applied Biosystems, USA) in a GeneAmp® PCR System 2720 Thermal Cycler (Applied Biosystems, USA) following the manufacturer's protocol. Table 1 represents the cycling conditions of RT-PCR and Table 2 presents the sequence primers, annealing, and detection temperature.

Real Time-PCR studies

Real-Time PCR reactions was conducted for E-cadherin gene inBioRad iCycler instrument (BioRad, CA, USA), using iQ™ Sybr® Green Supermix (BioRad, CA, USA) and 1 μl of the 10x diluted cDNA template in a total reaction volume of 10 μl. 18s rRNA gene served as the endogenous control. The RT reactions for each sample were carried out in triplicate to ensure best reproducibility. Negative controls without template were also accounted in each set of PCR assays. The expression analysis study was based upon the relative quantification method in which the change in

Table 1: Cycling conditions of RT-PCR

Step	Step 1	Step 2	Step 3	Step 4
Temperature (°C)	25	37	85	4
Time (min)	10	120	5	∞

RT-PCR = Reverse transcription polymerase chain reaction

Table 2: Primer sequences and cycling conditions for real time PCR

Genes	Expression primers and cycling conditions	Product size
18s rRNA	FP: GTAACCCGTTGAACCCCATT RP: CCATCCAATCGGTAGTAGCG Cycling: 95°C for 5 min (1 cycle), 95°C for 30 s, 55°C for 30 s, and 72°C for 30 s (40 cycles)	151 bp
E-cadherin	FP: CGGGAATGCAGTTGAGGATC RP: AGGATGGTGTAAGCGATGGC Cycling: 95°C for 5 min (1 cycle), 95°C for 30 s, 55°C for 30 s, 72°C for 30 s (40 cycles)	201 bp

PCR = Polymerase chain reaction, FP = Forward primer, RP = Reverse primer, bp = Base pair

mRNA level of a gene was relative to the levels of an internal control RNA (18S rRNA) that can be coamplified in the same PCR condition. The Ct value obtained for E-cadherin was normalized using the Ct values for 18S rRNA that yielded a ΔCt that was plotted for different IO doses. The relative quantification ($RQ = 2^{-\Delta\Delta Ct}$) value of the gene were then estimated that gave the fold changes. *P* value was determined using Student's *t*-test.

Semi-quantification of immunocytochemical expression of E-cadherin

Immunocytochemistry was performed for HaCaT cells of both control and experimental group using primary antibody for E-cadherin (clone EP700Y, Cat. No. ab40772, Abcam, Cambridge, UK) and fluorescein isothiocyanate (FITC) conjugated secondary antibody (goat polyclonal to rabbit IgG, Cat. No. ab6717, Abcam, Cambridge, UK; 1:500 in PBS). The cells were counterstained with 4',6-diamidino-2-phenylindole (DAPI; Sigma-Aldrich, USA) for visualization of nucleus. The expression of E-cadherin was semi-quantitatively evaluated by computing the grey scale intensity values of the membrane and cytoplasm from ICC images using AxioVision software (version 4.7.2, Carl Zeiss, Germany). Notch box plots were constructed using Matlab R2012b to compare the variation in E-cadherin -expression.

Bioelectrical characterization

HaCaT cells were seeded at a concentration of 10^4cells/ml in the commercially available ECIS slide (model no. 8W1E) from Applied Biophysics, USA and incubated overnight at 37°C and 5% CO_2. The confluent HaCaT cells were then exposed to different IO doses and incubated for 5 h. The bioelectrical characterization was performed at the initial time point and after 5 h. The electrical parameters viz

[Downloaded free from http://www.toxicologyinternational.com on Monday, October 10, 2016, IP: 115.115.223.222]

impedance magnitude (Z) and phase angle (Θ) over the frequency range of 100 Hz–100 kHz were measured with LCR meter (Hoiki, Japan).

Data analysis

Cell viability

The bar diagram for cell viability was prepared for MTT assay by computing the mean and standard deviation of the three replicates for each IO doses and using Microsoft Excel. Mean and standard deviation are given by the equation 1 and 2 mentioned below where,

$\bar{x}$: The mean; n: The number of data item;: $\sum x$ The sum of all data values and SD: Standard deviation

$$\bar{x} = \frac{\sum x}{n} \quad (1)$$

$$SD = \sqrt{\frac{\Sigma(x - \bar{x})}{n}} \quad (2)$$

Analysis of E-cadherin expression

The notch box plot was computed from the grey scale intensity value of E-cadherin intensity from ICC images of HaCaT after IO exposures. For each sample, grey scale intensity values were noted randomly selecting 50 points each for membranous as well as cytoplasmic E-cadherin expression. The notch box plot was computed using Matlab R2012b software.

Analysis of E-cadherin RT-PCR data

Bar diagram was plotted for studying variation in the level of mRNA expression in terms of ΔCt for E-cadherin expression with respect to the endogenous control 18S rRNA in HaCaT under exposures to different IO doses for 5 h. The level of significance for the differential expression of E-cadherin in HaCaT was evaluated by Student's *t*-test given by equation 3 where

$$t = \frac{X_1 - X_2}{\sqrt{\frac{S_1^2}{n_1} - \frac{S_2^2}{n_2}}} \quad (3)$$

$\bar{x}_1$= Mean of first set of values

$\bar{x}_2$= Mean of second set of values

S_1= Standard deviation of first set of values

S_2= Standard deviation of second set of values

n_1= Total number of values in first set

n_2= Total number of values in second set

Analysis of bioelectrical data:

Data on electrical impedance(Z) was taken in terms of its magnitude(|Z|) and phase angle(Θ) at different frequencies. The impedance spectroscopy data has been fitted with the magnitude and phase component of the expression of cell covered electrode given by equation 4 which has been developed by Giaever and Keese[31]

$$\frac{1}{z_c} = \frac{1}{z_n}\left(\frac{z_n}{z_n + z_m} + \frac{\frac{z_n}{z_n + z_m}}{\frac{\gamma r_c l_0(\gamma r_c)}{2l_1(\gamma r_c)} + 2R_b\left(\frac{1}{z_n} + \frac{1}{z_m}\right)}\right),$$

$$\gamma = \sqrt{\frac{\rho}{h}\left(\frac{1}{z_n} + \frac{1}{z_m}\right)} \quad (4)$$

where Z_c is the specific impedance of the cell covered electrode, Z_n is the specific impedance of the electrode electrolyte interface, Z_m is the specific cell impedance (= R_m-j/ωC_m), r_c is the effective cell radius, ρ is the resistivity of the medium, h is the average gap between the cell and the substrate, and R_b is the cell–cell junction resistance.

The fitting has been carried out using MATLAB 7.0 by Levenberg Marquardt algorithm method to extract the vital cell and medium parameters like the cell radius, cell–cell junction resistance, cell impedance, cell–substrate height, and medium resistivity with different IO concentration. The value of Z_n has been obtained from the impedance data in absence of cell.

Evaluation of biomechanical property by micropipette aspiration technique

The aspiration setup consisted of a micropositioner (MP-285, Sutter Inc) to position the glass pipette to the appropriate location under the microscope (I × 81, Olympus Inc) where the cell was expected to enter. A CCD camera (DP72, Olympus Inc) was attached to the microscope for the image capture. The cells were brought closer to the mouth of the pipette adjusting the XY stage present with the microscope. Once the cell was brought close to the pipette, suction pressure inside the pipette had been increased using the controller of the microinjector. This suction pressure generated inside the pipette helped in aspiration of the cell into the pipette. The resolution of the microinjector for the experiment was about 1 hPa (100 Pa) which is a limitation for extracting the mechanical properties of the cells in some cases. Thus, the used setup show the influence of IO doses on HaCaT, based on the suction force needed to initiate the aspiration of cell into the pipette. The value of the pressure was noted when the cell was just attached to the tip of the pipette and also at the point when it started entering the pipette. The difference

[Downloaded free from http://www.toxicologyinternational.com on Monday, October 10, 2016, IP: 115.115.223.222]

of these two applied pressures determines the suction force needed to aspirate the cell. The pipette used for this experiment was 5.7 μm in diameter. The resolution of the force with respect to the resolution of the microinjector was calculated based on the relation:

$$F = P \times \pi R_P^2$$

where P is the suction pressure and R_p is the inner radius of the pipette.

The value of the suction force that can be resolved is estimated to be about 2.58 nN. It is to be noted that the value of the force was assumed to be at a point, but the actual pressure that the cell experiences is distributed in nature.

RESULTS

Cell viability

PCM

The PCM microphotographs for HaCaT are shown in Figure 1a-d of control and experimental groups. Figure 1a exhibited confluent population of HaCaT in control groups. The confluency of HaCaT was noted to be remarkably affected with increased IO exposure. The effects were very prominent on exposure to 6 and 8% IO doses and dead cells were visible as white patch [Figure 1d].

MTT assay

MTT assay was performed to assess the mitochondrial functionality and cellular viability on exposure to different doses of IO for 5 h. Figure 2 showed the decreasing trend of mitochondrial functionality and viability of HaCaT with the increase in IO doses. The cell viability was expressed as percentage relative to the untreated control cells.

Relative quantification of E-cadherin expression

Relative quantification studies indicated differential impact of IO doses on the expression pattern of E-cadherin in HaCaT as shown in Figure3 after 5 h of exposures in 0, 4, 6, and 8% IO. A significant down regulation was noted in the expression of E-cadherin in comparison to that of the endogenous control 18S rRNA and the effect was found to be statistically significant in higher doses of 6% IO ($P = 0.002$*) and 8% IO ($P = 0.0001$*).

Semiquantification of immunocytochemical expression of E-cadherin

The immunocytochemical (ICC) observations confirmed remarkable changes in expression of E-cadherin in HaCaT on incubation with different doses of IO for 5 h. A loss of membranous E-cadherin expression was noted in HaCaT with concomitant increase in cytoplasmic site on exposure to IO doses and a complete membranous disruption for this molecule was noted at 8%. The semiquantification of membranous and cytoplasmic E-cadherin intensity for HaCaT was computed from the ICC images. The notch box plots for HaCaT [Figure 4] on exposure to various IO doses were plotted. It was observed that the membranous E-cadherin intensity decreased progressively with an increase in the cytoplasmic E-cadherin concentration on exposure to higher doses of IO.

Variation in electrical impedance over frequency domain

The impedance magnitude and phase with frequency has been plotted over the frequency range 100 Hz–100 kHz for HaCaT in different temporal points, that is, at initial and after 5 h of IO exposures [Figure 5a1, b1, a2, and b2]. The average ensembles of the electrical parameters of the cell and the surrounding medium which have been extracted by fitting Equation 1 with the experimental characteristics of Figure 5

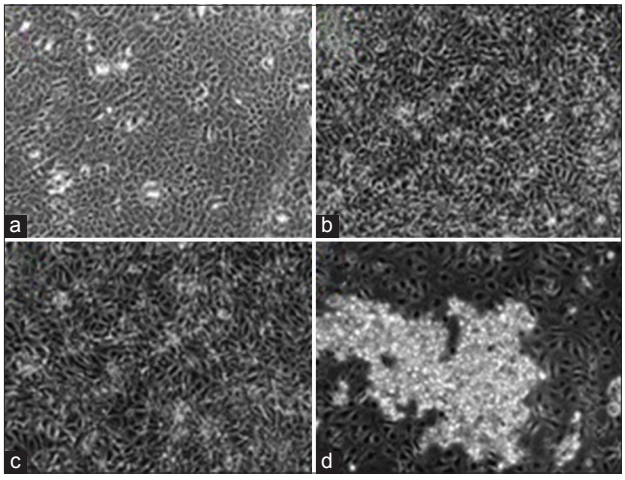


Figure 1: Phase-contrast microscopic images (× 10) ofHaCaT (a-d) cell of control and 5 h after exposure to iso-octane (IO) doses. In comparison to control (a), 4% (b), and 6% (c) IO groups; A large dead cell population (white patches) is noted for 8% (d) IO group along with visible increase in intercellular space of HaCaT

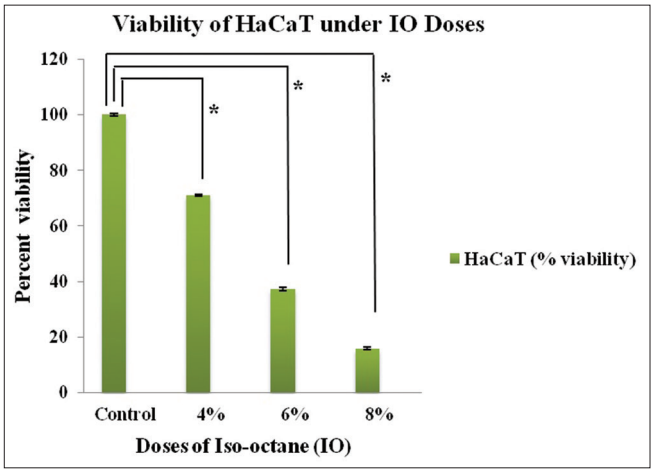


Figure 2: Bar diagram representing the 3-(4,5- dimethylthiazol-2-yl)-2, 5-diphenyl-2H- tetrazolium bromide (MTT) assays of HaCaT after treatment with different IO doses for 5 h. The relative cell viability expressed as a percentage relative to the control. Bars represented steep decrease in cellular functional vitality. *Represent $P < 0.05$

[Downloaded free from http://www.toxicologyinternational.com on Monday, October 10, 2016, IP: 115.115.223.222]

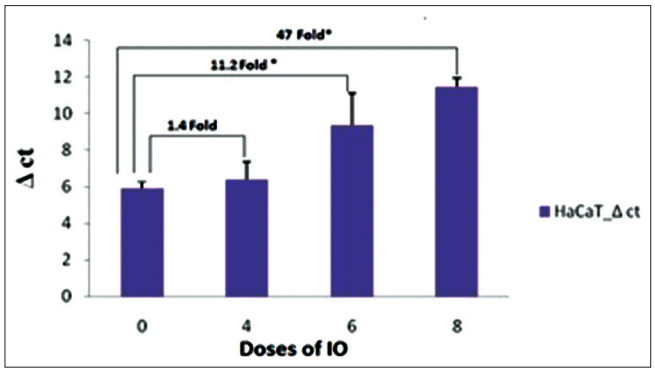


Figure 3: Comparison of E-cadherin expression. Bar graphs represent ΔCt values of E-cadherin expression with respect to that of 18S rRNA in HaCaT under chemical assaults at different IO concentration. *Indicates the differences that are statistically significant ($P < 0.05$)

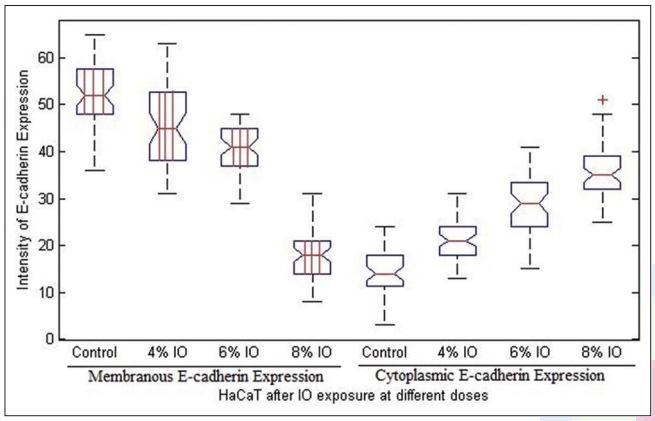


Figure 4: Notch box plot depicting membranous and cytoplasmic E-cadherin intensity of HaCaT under IO exposure

are shown in Table 3 along with the fit quality factor (qf). It was observed from Figure 5a1 that the impedance magnitude of 0% (control) and 4% IO were very close and that of 6 and 8% IO decreased significantly above 300 Hz in the initial stage. However, the phase angle differed even at 4% IO dose and the magnitude of the phase angle decreased with increasing dose of IO as observed from Figure 5a2. This may be attributed to the fact that the effective capacitive impedance decreased and the resistive component increased and the capacitive impedance dominated the overall magnitude.

This may be partially explained from the R_m and C_m parameters in Table 3 which suggested that the contribution of the capacitive impedance of the cell was more prominent than the resistive component and the capacitive impedance decreased with increasing IO dose. After 5 h, the impedance was lower than that in the initial condition and decreased continuously with frequency over the entire range and that the impedance for 6 and 8% IO dose was significantly lower than 0% [Figure 5b1]. This may be explained from Table 3 that all the resistive parameters like the cell–cell junction resistance, and medium resistivity decreased. But the phase angle for 4–8% IO dose did not change significantly after 5 h [Figure 5b2]. This may be attributed to the fact that the effective resistive component of the impedance decreased and the capacitive impedance also increased, thus reducing the net change.

Biomechanical characterization of HaCAT under IO exposures

Analysis of biomechanical properties of HaCaT by

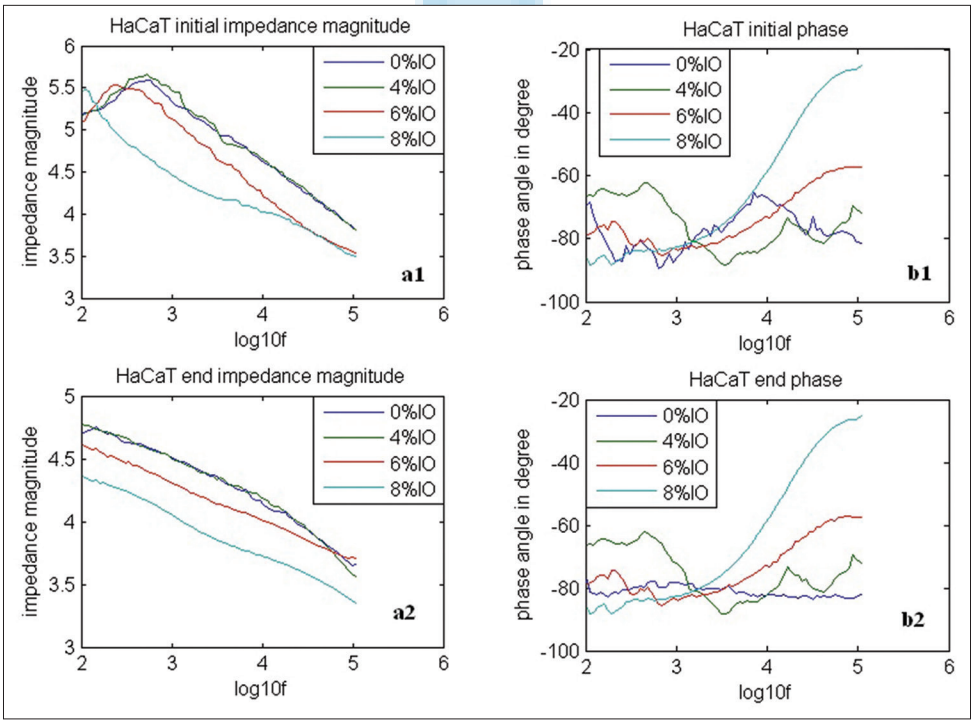


Figure 5: Plot of logarithmic value electrical impedance (z) magnitude and phase over the frequency (f) range of 100 Hz–100kHz of HaCaT at initial (a1 and b1) and final (a2 and b2) state of the experiment on exposure to different doses of IO (0, 4, 6, and 8%)

[Downloaded free from http://www.toxicologyinternational.com on Monday, October 10, 2016, IP: 115.115.223.222]

Table 3: Fitted parameter from the impedance spectroscopy data

Parameters	Initial condition (different IO doses)				Final (after 5 h; different IO doses)			
	0%	4%	6%	8%	0%	4%	6%	8%
R_b (Ωcm^2)	10	9.8	7.5	4.5	9.95	8.5	2	1
r_c (μm)	15	15	15	15	15	15	12	10
H (nm)	50	51.2	58.5	70	50.5	55	68	100
R_m (Ωcm^2)	0.5	0.5	0.5	0.5	0.45	0.48	0.44	0.3
C_m ($\mu F/cm^2$)	1.1	1.2	2.0	3.5	1.3	3.5	5	8
P (Ωcm)	150	150	150	150	140	110	60	20
Qf (quality factor)	0.001	0.0012	0.0011	0.0012	0.0013	0.001	0.0012	0.0012

Table 4: Change in HaCaT stiffness on 5 hincubation with IO doses

Cell type	IO doses	Suction force (nN)	Remarks on the deformation characteristic of the cell's membrane
HaCaT	Control	≤2.58	Cells entered the micropipette in a long cylindrical shape but regained the original form on release (Figure 6a)
	4%	≤2.58	Cellsentered the micropipette with a hemispherical cap but regained the original shape slowly on release (Figure 6b)
	6%	15.48±7.75	Cell membrane manifested damage on application of suction force and could not enter the micropipette even after increasing the suction force for several times in comparison to control (Figure 6c)
	8%	≤2.58	Initially cells entered the micropipette with a long cylindrical shape having hemispherical cap on application of suction force equal to that for control and 4% groups. But on release entire cell membrane burst open (Figure 6d)

micropipette aspiration techniqueis given in Table 4. It may be noted from Table 4 that there is no difference in the suction force in case of control and the cells treated with 4% IO. This is to be attributed to the resolution of the force that can be measured using the setup. However, the deformation characteristic of the cell changes on exposure to 4% IO. It was observed that the normal HaCaT entered the micropipette with a cylindrical shape [Figure 6a] on application of minimum suction force [Table 4] and readily regained the original shape on release. But under exposure to IO doses such biomechanical property was altered [Table 4]. The HaCaT cells gradually became stiff and then fragile particularly in high doses. Therefore, under 4% IO, cells entered the micropipette forming a hemispherical cap [Figure 6b], but after release it took time to regain the original shape. However, on treatment with 6% IO cells manifested localized membrane damage on application of suction force and could not enter into the micropipette even after increasing the suction force more than several times to that of control [Figure 6c]. Interestingly, under 8% IO the cells though initially entered the micropipette with a long cylindrical shape

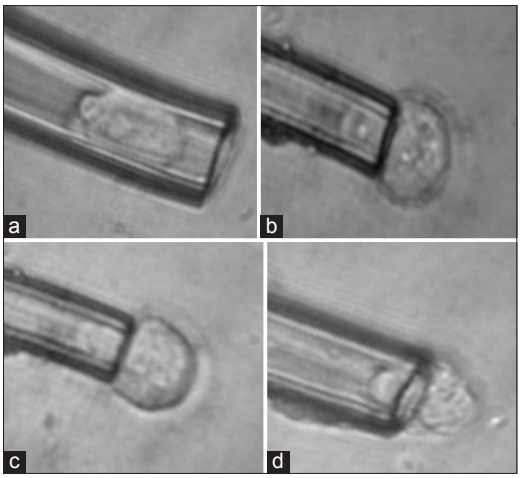


Figure 6: Phase-contrast microscopic view of micropipette aspiration of HaCaT. (a) Control group and (b-d) experimental groups on incubation with 4, 6, and 8% IO for 5 h, respectively

on application of suction force equal to that for control and 4% groups; but on release, the entire cell membrane bursts open [Figure 6d].

DISCUSSION

The present investigation explored the dose-dependent effects of IO on structural and functional aspects of HaCaT cells through various bioassays. Further the study has been extended to characterize the bioimpedance and biomechanical proprieties of the cells undergoing IO treatment and the observations have been correlated with the bioassay results. The MTT assays provided the information about the degree of toxicity of IO doses on HaCaT as revealed from Figure 2. Under such chemical assault the cells became stressed which increase further under higher doses and alteration in its morphological structure as well as disruption of cellular association had been induced.[13] The disruption in cellular association was manifested at the molecular level demonstrated by transcriptomic down regulation of E-cadherin and its dislocation from membranous sites in HaCaT under IO doses [Figures 3 and 4]. The above study is comparable with the published literature[15] which signified that the disruption in epithelial cell–cell association could be due to reduction in membranous E-cadherin expression. This disruptive effect of IO was further assessed at the level of bioelectrical properties. This biological understanding on cellular status is known to bear significance in evaluating cytotoxicity effects of various chemicals.[16,17] When cellular biochemical pathways are affected the electrical properties of cells also get modified which may be detected much earlier than the altered chemical properties.[20,21] The distinct difference in the impedance characteristics under IO exposures at initial and final point as observed in Figure 5 clearly illustrated the toxic impact on the

[Downloaded free from http://www.toxicologyinternational.com on Monday, October 10, 2016, IP: 115.115.223.222]

electrical properties of the cell line. Here, it may be noted that the membrane permeability of HaCaT was affected due to disruption of membranous E-cadherin as revealed through immunocytochemical observation [Figure 4], and thus possibly resulted the change in the cellular electrical bioimpedance. Hence, it may be stated that the distinct observations in Table 3 on the change in the electrical parameters which was more significant with 6 and 8% IO doses were also corroborative with the findings on E-cadherin down regulations [Figures 3 and 4]. Further the reduction in the value of cell–cell function resistance (r_b) with increasing doses of IO, particularly after 5 h of assaults could be associated with cellular viability status. This finding was plausibly attributed to the fact that the cells become dead and get detached from one another [Figure 1], thereby increasing their effective cross-sectional area and resulting the fall in cell–cell junction resistance. Furthermore, disruption of membranous E-cadherin at higher IO doses could be connoted with the decrease in the capacitive impedance. The cell death phenomena and subsequently their separation from each other as well as from substrate was increasing, which was supported by the higher value of h parameter obtained from the fittings of impedance results. Supportive observation on cellular spatial features were noted under PCM and cell viability assay. The increase of C_m and decrease of R_m values may be attributed to the reduction of the membranous E-cadherin expression with increased IO dose leading to a possible membrane disruption as indicated in Figure 5. The above phenomenon might lead to the reduction of effective cellular impedance. Furthermore, the disruption of membrane integrity along with destructive cellular activities can lead to the release of ions into the surrounding medium, resulting in a reduction of effective resistivity as observed from Table 3. Thus, it may be inferred that the electrical results further strengthen the microscopic and molecular observations in this study.

The analysis of biomechanical properties of cells by micropipette aspiration is a versatile method to understand the material and biophysical properties of living cells.[29] In micropipette aspiration experiment, it has been observed that HaCaT cell can easily change its shape to fit in a specific location on application of external forces and regains its original shape immediately on withdrawal of the forces. This was possible because normal cells were quite flexible due to its viscoelastic properties.[30] However, under exposure to IO doses, the biomechanical properties of HaCaT cells were modified due to alteration of its biochemical characteristics including membrane features as demonstrated through E-cadherin findings. The HaCaT cells gradually became stiffer and fragile particularly under high doses of IO. Under 4% IO, cells took time to regain its original shape on release of external forces. For 6% IO dose, cell manifested severe membrane damage, and thus it was difficult to aspirate even after application of much higher suction force as observed in Figure 6c. Interestingly it was observed that under 8% IO, although the cells could be easily aspirated, but on release they burst open [Figure 6d]. It was mostly due to extreme fragility of the cells under higher IO exposure. This biomechanical alteration is supposed to be corroborative with the down regulation in E-cadherin expression and its dislocation from membranous site with the increase of IO doses. Furthermore, it may be stated that when cells were subjected to more percentage of IO, the morphological deformations became less reversible, implying remarkable change in biomechanical properties of these biological entities. Considering cutaneous irritational impact of IO and insufficiency in the related biological data, present study has explored the various effects of this OS on epithelial cells (HaCaT) *in vitro*. The study thus involved structural, molecular, bioelectrical, and biomechanical characterization of HaCaT cells under IO exposures; and tried to correlate their results for evaluation of the cytotoxicity. Thus, it may be concluded that this study has successfully validated the toxic effects of IO doses on epithelial cell at structural and functional levels and elucidated that 8% IO dose is lethal for this cell population.

Acknowledgements

Financial support through the National Program on Micro and Smart Systems (NPMASS), Govt of India, for this study, is greatly acknowledged. We also extend our heartiest thanks to Prof. Ananthasuresh G K, Santosh D B Bhargav, Sajeesh Kumar M P, and Shilpa Raju R, Dept. of Mechanical Engineering, Indian Institute of Science, Bangalore for providing infrastructural support in mechanobiological experiment in this study. Authors are thankful to Dr. Sanghamitra Sengupta and Mrs Sanmitra Basu of Dept. of Biochemistry, Calcutta University for providing infrastructural support in PCR studies. Authors greatly acknowledge the support of Dr. Chirosree Roy Chaudhuri of Bengal Engineering and Science University, Shibpur, Howrah for the bioelectrical studies.

Financial support and sponsorship

Nil.

Conflicts of interest

There are no conflicts of interest.

REFERENCES

1. Official Journal of the European Union 2006;396:849.
2. Bushnell PJ, Boyes WK, Shafer TJ, Bale AS, Benignus VA. Approaches to extrapolating animal toxicity data on organic solvents to public health. Neurotoxicology 2007;28:221-6.
3. Tanford C. The Hydrophobic Effect: Formation of Micelles and Biological Membranes; 2nd ed. New York: J. Wiley; 1980.
4. Tanford C. Protein denaturation. Theoretical models for the mechanism of denaturation. Adv Protein Chem 1970;24:1-9.

[Downloaded free from http://www.toxicologyinternational.com on Monday, October 10, 2016, IP: 115.115.223.222]

5. Werner D, Arno R, Andrea S, Klaus R. Automotive Fuels in Ullmann's Encyclopedia of Industrial Chemistry. Weinheim: Wiley-VCH; 2007. doi:10.1002/14356007
6. Totten GE, Westbrook SR, Shah RJ. Fuels and lubricants handbook: Technology, properties, performance and testing. West Conshocken: ASTM International; 2003.
7. Schellman JA. Solvent denaturation. Biopolymers 1978;17:1305-22.
8. Miura S, Zou W, Ueda M, Tanaka A. Screening of genes involved in isooctane tolerance in Saccharomyces cerevisiae by using mRNA differential display. Appl Environ Microbiol 2000;66:4883-9.
9. Visvader JE. Cells of origin in cancer. Nature 2011;469:314-22.
10. Cannava A, Ceci P, Coletti D, Cortesi M, Papa F, Vivarelli E, *et al*. Toxic effects of polychlorinated biphenyls in myogenic cells. J Health Sci 2003;50:33-41.
11. Schrand AM, Rahman MF, Hussain SM, Schlager JJ, Smith DA, Syed AF. Metal-based nanoparticles and their toxicity assessment. Nanomed Nanobiotechnol 2010;2:544-68.
12. Wang L, Nagesha DK, Selvarasah S, Dokmeci MR, Carrier RL. Toxicity of CdSe Nanoparticles in Caco-2 Cell Cultures. J Nanobiotechnol 2008;6:11.
13. Pujalte I, Passagne I, Brouillaud B, Tréguer M, Durand E, Courtès CO, *et al*. Cytotoxicity and oxidative stress induced by different metallic nanoparticles on human kidney cells. Part Fibre Toxicol 2011;8:10.
14. Jakob T, Brown MJ, Udey MC. Characterization of E-cadherin containing junctions involving skin-derived dendritic cells. J Invest Dermatol 1999;112:102-8.
15. Yamada S, Pokutta S, Drees F, Weis WI, Nelson JW. Deconstructing the cadherin-catenin-actin complex. Cell 2005;123:889-901.
16. Heijink IH, Kies MP, Kauffman HF, Postma DS, Oosterhout AJ, Vellenga E. Down-regulation of E-cadherin in human bronchial epithelial cells leads to epidermal growth factor receptor-dependent Th2 cell-promoting activity. J Immunol 2007;178:7678-85.
17. Charman RA. Introduction Part I: The Electric Cell. Physiotherapy 1990;76:502-8.
18. Charman RA. Part III: Bioelectrical potentials and tissue currents. Physiotherapy 1990;76:643-54.
19. Prozialeck WC, Lamar PC. Cadmium (Cd2+) disrupts E-cadherin-dependent cell-cell junctions in MDCK Cells". *In Vitro* Cell Dev Biol Anim 1997;33:516-26.
20. Killion JJ. Electrical Properties of normal and transformed mammalian cells. Biophys J 1990;45:523-8.
21. Asphahani F, Thein M, Veiseh O, Edmondson D, Kosai R, Veiseh M, *et al*. Influence of cell adhesion and spreading on impedance characteristics of cell-based sensors. Biosens Bioelectron 2008;23:1307-13.
22. Davey CL, Markx GH, Kell DB. On the dielectric method of monitoring cellular viability. Pure Appl Chem 1993;65:1921-6.
23. Bao N, Wang J, Lu C. Recent advances in electric analysis of cells in microfluidic systems. Anal Bioanal Chem 2008;391:933-42.
24. Brouard M, Casado M, Djelidi S, Barrandon Y, Farman N. Epithelial sodium channel in human epidermal keratinocytes: Expression of its subunits and relation to sodium transport and differentiation. J Cell Sci 1999;112:3343-52.
25. Chakraborty PK, Lee WK, Molitor M, Wolff NA, Thévenod F. Cadmium induces Wnt signaling to upregulate proliferation and survival genes in sub-confluent kidney proximal tubule cells. Mol Cancer 2010;9:102.
26. Janmey PA, Kinnunen PK. Biophysical properties of lipids and dynamic membranes- Special issue: Membrane Dynamics. TRENDS in Cell Biology; 2006.
27. Faffe DS, Zin WA. Lung parenchymal mechanics in health and disease. Physiol Rev 2009;89:759-75.
28. Wyss K, Yip CY, Mirzaei Z, Jin X, Chen JH, Simmons CA. The elastic properties of valve interstitial cells undergoing pathological differentiation. J Biomech 2012;45:882-7.
29. Suresh S, Spatz J, Mills JP, Micoulet A, Dao M, Lim CT, *et al*. Connections between single-cell biomechanics and human disease states: Gastrointestinal cancer and malaria. Acta Biomater 2005;1:15-30.
30. Wu ZZ, ZhangG, Long M, Wang HB, Song GB, Cai SX. Comparison of the viscoelastic properties of normal hepatocytes and hepatocellular carcinoma cells under cytoskeletal perturbation. Biorheology 2000;37:279-90.
31. Giaever I and Keese CR. Micromotion of mammalian cells measured electrically. Proc. Natl Acad Sci USA 1991;88:7896-900.